

This is a repository copy of *Photolysis driven indoor air chemistry following cleaning of hospital wards*.

White Rose Research Online URL for this paper:  
<https://eprints.whiterose.ac.uk/161639/>

Version: Published Version

---

**Article:**

Carslaw, Nicola [orcid.org/0000-0002-5290-4779](https://orcid.org/0000-0002-5290-4779) (2020) Photolysis driven indoor air chemistry following cleaning of hospital wards. *Indoor air*. INA-19-11-338.R2. ISSN 0905-6947

<https://doi.org/10.1111/ina.12702>

---

**Reuse**

This article is distributed under the terms of the Creative Commons Attribution (CC BY) licence. This licence allows you to distribute, remix, tweak, and build upon the work, even commercially, as long as you credit the authors for the original work. More information and the full terms of the licence here:  
<https://creativecommons.org/licenses/>

**Takedown**

If you consider content in White Rose Research Online to be in breach of UK law, please notify us by emailing [eprints@whiterose.ac.uk](mailto:eprints@whiterose.ac.uk) including the URL of the record and the reason for the withdrawal request.



# Photolysis-driven indoor air chemistry following cleaning of hospital wards

Zixu Wang<sup>1</sup> | Shawn F. Kowal<sup>2</sup> | Nicola Carslaw<sup>1</sup> | Tara F. Kahan<sup>2,3</sup>

<sup>1</sup>Department of Environment and Geography, University of York, York, UK

<sup>2</sup>Department of Chemistry, Syracuse University, Syracuse, NY, USA

<sup>3</sup>Department of Chemistry, University of Saskatchewan, Saskatoon, SK, Canada

## Correspondence

Nicola Carslaw, Department of Environment and Geography, University of York, York, UK.

Email: nicola.carslaw@york.ac.uk

Tara F. Kahan, Department of Chemistry, Syracuse University, Center for Science and Technology, Syracuse, NY 13244, USA.

Email: tara.kahan@usask.ca

## Present address

Shawn F. Kowal, Ecology and Environment, Lancaster, NY, USA

## Funding information

Alfred P. Sloan Foundation, Grant/Award Number: G-2017-9796 and G-2018-11062

## Abstract

Effective cleaning techniques are essential for the sterilization of rooms in hospitals and industry. No-touch devices (NTDs) that use fumigants such as hydrogen peroxide (H<sub>2</sub>O<sub>2</sub>), formaldehyde (HCHO), ozone (O<sub>3</sub>), and chlorine dioxide (OCIO) are a recent innovation. This paper reports a previously unconsidered potential consequence of such cleaning technologies: the photochemical formation of high concentrations of hydroxyl radicals (OH), hydroperoxy radicals (HO<sub>2</sub>), organic peroxy radicals (RO<sub>2</sub>), and chlorine radicals (Cl) which can form harmful reaction products when exposed to chemicals commonly found in indoor air. This risk was evaluated by calculating radical production rates and concentrations based on measured indoor photon fluxes and typical fumigant concentrations during and after cleaning events. Sunlight and fluorescent tubes without covers initiated photolysis of all fumigants, and plastic-covered fluorescent tubes initiated photolysis of only some fumigants. Radical formation was often dominated by photolysis of fumigants during and after decontamination processes. Radical concentrations were predicted to be orders of magnitude greater than background levels during and immediately following cleaning events with each fumigant under one or more illumination condition. Maximum predicted radical concentrations (1.3 × 10<sup>7</sup> molecule cm<sup>-3</sup> OH, 2.4 ppb HO<sub>2</sub>, 6.8 ppb RO<sub>2</sub> and 2.2 × 10<sup>8</sup> molecule cm<sup>-3</sup> Cl) were much higher than baseline concentrations. Maximum OH concentrations occurred with O<sub>3</sub> photolysis, HO<sub>2</sub> with HCHO photolysis, and RO<sub>2</sub> and Cl with OCIO photolysis. Elevated concentrations may persist for hours after NTD use, depending on the air change rate and air composition. Products from reactions involving radicals could significantly decrease air quality when disinfectants are used, leading to adverse health effects for occupants.

## KEYWORDS

disinfection, fluorescent light, indoor air quality, photochemistry, sunlight

Carslaw and Kahan should be considered joint senior authors.

The peer review history for this article is available at <https://publons.com/publon/10.1111/ina.12702>

This is an open access article under the terms of the Creative Commons Attribution-NonCommercial-NoDerivs License, which permits use and distribution in any medium, provided the original work is properly cited, the use is non-commercial and no modifications or adaptations are made.

© 2020 The Authors. *Indoor Air* published by John Wiley & Sons Ltd



reduce bacteria counts to safe levels, and safety concerns have focused on the toxicity of the cleaning agents.<sup>41-48</sup> However, health effects from reactions involving these fumigants have not been considered. The potential for secondary reactions or indoor photolysis of these gases to produce radicals, which can further react to form potentially harmful species, has also not been considered.

In the outdoor environment, photochemical reactions produce hydroxyl (OH), hydroperoxy (HO<sub>2</sub>), organic peroxy (RO<sub>2</sub>), and chlorine (Cl) radicals, which can react to form a wide range of species in the atmosphere (Figure 1). Indoors in the absence of strong sunlight and washout, these oxidized species can have much longer lifetimes, which is of concern given some of them have negative health impacts.<sup>49</sup> Oxidant reactions with many common indoor species can produce particulate matter (PM), which can irritate airways, exacerbate existing pulmonary conditions such as asthma, and even cause premature death in vulnerable people.<sup>50-53</sup>

Light indoors (either artificial sources or sunlight filtered through closed windows) does not typically contain photons at the short wavelengths (290-330 nm) responsible for most photolysis outdoors (Figure 2). Traditionally, indoor photolysis was not considered an important indoor source of oxidants, though recent work demonstrated that indoor light sources can emit at wavelengths as short as 300 nm and that compounds such as nitrous acid (HONO), HCHO, Cl<sub>2</sub>, and HOCl can photolyze under irradiation from indoor lights to generate radicals,<sup>54-58</sup> thereby increasing the oxidizing capacity of air indoors. During cleaning events with NTDs, concentrations of the photolabile disinfecting molecules are very high relative to outdoors. It is possible that photolysis of the disinfectant gases during and after cleaning events could form significant radical concentrations, leading to previously unconsidered adverse health effects.

The aim of this paper is to investigate radical behavior indoors during and after simulated NTD cleaning events using O<sub>3</sub>, OCIO, HCHO, and H<sub>2</sub>O<sub>2</sub>. We focus mainly on the primary radicals (ie, those formed directly from photolysis), but also include RO<sub>2</sub> radicals given they coexist with other radical species and can contribute to OH formation. We use photolysis rate constants to calculate the formation

rates of OH, HO<sub>2</sub>, and Cl and a detailed chemical model to investigate radical behavior during the use of these technologies and under different lighting conditions. Steady-state radical concentrations were determined for peak disinfectant levels, as well as at the times when disinfectant levels decreased to the short- and long-term exposure limits and to background levels.

## 2 | METHODS

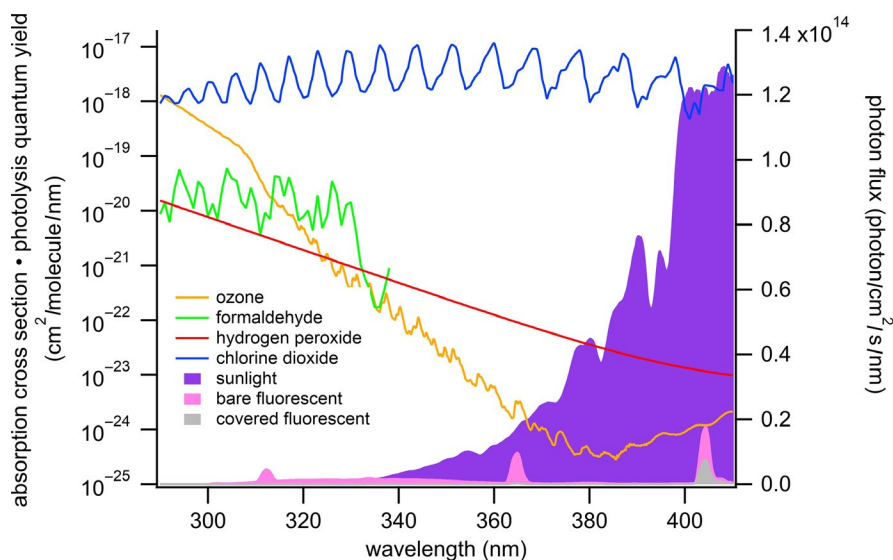
### 2.1 | Model

Concentrations of each disinfectant, radical species, and other indoor trace gases were calculated using the INDCM (INdoor Detailed Chemical Model).<sup>59-61</sup> The INDCM is a detailed chemical box model with a chemical scheme based on a comprehensive chemical mechanism (the Master Chemical Mechanism, MCM v3.2),<sup>62</sup> which includes around 20,000 reactions and 5,000 species representing the near-explicit degradation of ~143 VOCs (volatile organic compounds) in the gas phase.<sup>63-66</sup> The reaction of each VOC with OH, NO<sub>3</sub>, and O<sub>3</sub>, and photolysis where relevant, is the first step in the oxidation chain generating products including RO (oxy), RO<sub>2</sub> (peroxy), and RRCOO (criegee) radicals and continuing until the final oxidation products of CO<sub>2</sub> and H<sub>2</sub>O are formed. Additional reactions describe surface loss by deposition, VOC emission rates, partitioning between indoor gas and particle phases and exchange of species with outdoors, all of which have been described in detail in previous work.<sup>59,61</sup> For this work, the model described in Wong et al (2017)<sup>67</sup> for chlorine cleaning was adapted through the addition of reactions to account for OCIO chemistry (see Supporting Information), with rate coefficients from the IUPAC recommendations.<sup>68</sup>

The INDCM assumes a single well-mixed environment, and Equation 1 is used to calculate the concentration of each model species:

$$\frac{dC_i}{dt} = -V_d \left( \frac{A}{V} \right) C_i + \lambda_r f C_o - \lambda_r C_i + \frac{Q_i}{V_i} + \sum_{j=1}^n R_{ij} \quad (1)$$

**FIGURE 2** Photon fluxes 1 m from a sunlit window or fluorescent light bulbs in an office<sup>54</sup> and the product of absorption cross sections and photolysis quantum yields for radical precursors O<sub>3</sub>, H<sub>2</sub>O<sub>2</sub>, HCHO, and OCIO in the actinic region.<sup>78,83-85</sup> The H<sub>2</sub>O<sub>2</sub> trace is adapted from Ref. 54 based on interpolation from measured cross sections.<sup>78,85</sup>



where  $C_i$  ( $C_o$ ) is the indoor (outdoor) concentration of species  $i$ ,  $v_d$  its deposition velocity,  $A$  the surface area indoors,  $V$  the volume of air in the indoor environment,  $\lambda_r$  the air change rate between indoors and outdoors (ACR),  $f$  the building filtration factor,  $Q_i$  the indoor emission rate for species  $i$ , and  $R_{ij}$  the reaction rate between species  $i$  and  $j$ . The model can be initialized for global location, the type of indoor space (such as a hospital ward), outdoor pollutant concentrations, the time of year, and for consideration of occupant activities such as cleaning.

The INDCM includes terms that represent both indoor and attenuated outdoor lighting, which are added together to give the total photolysis rate.<sup>59,67</sup> We used the method described in this section for all 37 species in the model that undergo photolysis, with the exception of the four disinfectant gases under investigation (see next section). For indoor light sources, constant transmission of light was assumed between 300-400 nm (UV) and 400-700 nm (visible) according to the method developed by Nazaroff and Cass (1986)<sup>69</sup> and used as described by Carslaw (2007).<sup>59</sup> The photolysis rates outdoors were calculated using a 2-stream scattering model,<sup>70</sup> which assumed a typical mid-latitude value for ozone column and clear skies. Sunlight is attenuated as it passes through windows, such that 3 and 10%, respectively, of UV and visible light ingresses.<sup>59</sup>

The INDCM includes irreversible surface loss, but does not consider the release of gas-phase products from heterogeneous reactions. Currently, there are not enough data regarding heterogeneous reactions on indoor surfaces to parameterize the model effectively.

## 2.2 | Hospital ward conditions in the model

We assume a ward volume of 35 m<sup>3</sup> with an area to volume ratio of 1 m<sup>2</sup>/m<sup>3</sup>, the latter being similar to the laboratory setting studied in Wong et al.<sup>67</sup> Internal temperature was assumed to be 293 K and 50% relative humidity. Temperature and relative humidity could affect some of the chemistry modeled in this work, but we did not investigate the effects of changing these variables in this study, since there are many potential sources of uncertainty in the processes we investigate. The aim of this study is to demonstrate that photolysis of gaseous fumigants used to disinfect hospitals could occur under common indoor conditions, and to predict general conditions (lighting source, time after disinfection) under which the concentrations of radicals generated from photolysis will be elevated enough to affect indoor air quality.

Outdoor VOC concentrations were initialized based on Sarwar et al.,<sup>71</sup> while annual mean values of CO, SO<sub>2</sub>, NO, and NO<sub>2</sub> (250, 0.6, 2.7 and 13.5 ppb, respectively) from west Toronto/downtown were used to initialize the model (OMECC, 2016) following Wong et al.<sup>67</sup> Under baseline conditions, internal O<sub>3</sub>, NO, and NO<sub>2</sub> concentrations were approximately 30 ppb, 80-130 ppt (higher with more light), and 8 ppb, respectively, averaged from 09:00 h to 17:00 h.

Typical air change rates of ~6.5 /h for regular outpatient rooms in hospitals have been reported.<sup>72</sup> This change rate included recirculation: The exchange rate with outdoor air was ~2 per hour. We therefore used the air change rate of 2 per hour. The model results were similar even if we used 6.5 per hour, given that the ventilation is assumed

to be off when fumigant emission occurs. Ventilation was stopped in the model at 10:00 h, and the emission from the NTD was assumed to begin. The emissions were set to provide the approximate concentrations reported in the literature for NTD use: 25 ppm for ozone,<sup>73,74</sup> 1000 ppm for formaldehyde,<sup>30,31,33</sup> 100-500 ppm for H<sub>2</sub>O<sub>2</sub>,<sup>47,75</sup> and 3000 and 350 ppm for OCIO (to reflect two commonly used concentrations).<sup>30,76</sup> This required emission rates of 0.01 ppm/s to generate 25 ppm of O<sub>3</sub>, 0.5 ppm/s for 1000 ppm of HCHO, 0.3 ppm/s for 500 ppm of H<sub>2</sub>O<sub>2</sub>, and 0.8 and 0.1 ppm/s to deliver 3000 and 350 ppm of OCIO (see Supporting Information). The emission rates were set to achieve these concentrations in the dark, and we used the same emission rate for all lighting conditions for each individual gas. The emissions were assumed to last for one hour and then stop. After another hour (at noon), ventilation was resumed at 2 per h. There is very little information in the literature on how long the gases will be emitted during cleaning; there is no standard practice. The little information that exists suggests that emissions could last from between 30 minutes and 24 hours.<sup>30</sup> Duration of cleaning and ventilation regime afterward will obviously affect the results, but our assumption allows the reader to see the impact of one hour of cleaning at typical concentrations. Additionally, we note that outdoor air composition will only affect indoor air composition during periods when the ventilation is running (ie, before 10:00 am, when NTD emission commenced, and after 12:00 pm). Four lighting scenarios were considered in this study: no illumination (dark); light either from a covered fluorescent (CF) or bare fluorescent (BF) tube; and from a combination of CF and attenuated sunlight (ATT). Covered and bare fluorescent tubes are both common in non-residential buildings. As shown in Figure 2, bare fluorescent tubes emit at shorter wavelengths than indoor sunlight, due to filtering of ultraviolet light by windows. Conversely, emission at wavelengths shorter than ~360 nm is almost completely attenuated by plastic covers. For the 4 disinfectant (and 2 related) gases, photolysis rates were calculated using measured photon fluxes 1 m from each light source or the window for sunlight (Tables 1-4, Table S1). Sensitivity tests were also performed at a distance of 25 cm from the lightbulb, since the photon flux is expected to be 4.5× greater than at 100 cm.<sup>54</sup> We discuss the implications of these tests in the Implications section. Literature values of absorption cross sections ( $\sigma$ ) and photolysis quantum yields ( $\phi$ ) of O<sub>3</sub>, H<sub>2</sub>O<sub>2</sub>, HCHO, and OCIO were used, with photon fluxes ( $F$ ) from Kowal et al.<sup>54</sup> to calculate photolysis rate constants ( $J$ ) across the wavelength ( $\lambda$ ) range of interest using Equation 2:

$$J = \int_{\lambda_1}^{\lambda_2} \sigma(\lambda) \phi(\lambda) F_{\lambda} d\lambda \quad (2)$$

## 2.3 | Radical production rates

Radical production rates were calculated from Equations 3-6 using estimated baseline concentrations of H<sub>2</sub>O<sub>2</sub>, HCHO, O<sub>3</sub>, and OCIO in the absence of cleaning, as well as the short- and long-term exposure limits for each gas. The calculations used to determine the coefficients in Equations 3-5 are provided in Ref 54. The yields for ozone photolysis were adjusted to match the higher humidity (90-95%) required during cleaning events.<sup>31,38,77</sup> Quantum yields for OCIO and

ClO photolysis are assumed to be unity and 0.8 for Cl production from ClOOCl.<sup>78</sup>

$$\text{Rate} = 2J_{\text{H}_2\text{O}_2} [\text{H}_2\text{O}_2] \quad (3)$$

$$\text{Rate} = 2J_{[\text{rad}]}} [\text{HCHO}] \quad (4)$$

$$\text{Rate} = 0.31J_{[\text{O}(^1\text{D})]} [\text{O}_3] \quad (5)$$

$$\text{Rate} = J_{[\text{OCIO}]} [\text{OCIO}] \quad (6)$$

These calculations predict the rate at which primary radicals will be generated during cleaning events, regardless of secondary reactions and loss processes. Radical production rates and steady-state concentrations are reported at times when disinfectant gas concentrations were at their peaks, at long- and short-term exposure limits, and at background levels.

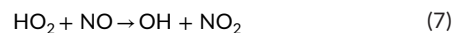
### 3 | RESULTS AND DISCUSSION

#### 3.1 | Baseline conditions

In the absence of cleaning, the primary oxidant precursors indoors will be O<sub>3</sub>, HONO, and HCHO. In our model, these are present at concentrations of 30, 0.5, and 2.6 ppb, respectively. Under these conditions, ozone-alkene reactions will be the primary OH source, with a formation rate on the order of 10<sup>7</sup> molecules/cm<sup>3</sup>/s.<sup>49</sup> Individual alkene concentrations and OH production rates used to calculate this rate are provided in the Supporting Information. Formaldehyde photolysis under illumination by BF will form HO<sub>2</sub> at a rate of ~1 × 10<sup>5</sup> molecules/cm<sup>3</sup>/s.<sup>54</sup> The main source of Cl in the absence of perturbations such as cleaning will be physical transport from outdoors; at an ACR of 2 per hour, we calculate a negligible indoor formation rate of ~6 × 10<sup>2</sup> molecules/cm<sup>3</sup>/s.

To further investigate the baseline conditions, the model was run without any emissions of the disinfectant gases to investigate the impact of outdoor pollutants and the ventilation regime (switched off for 2 hours from 10:00 h) for the simulations in isolation. Figure 3 shows the trends of HO<sub>2</sub>, OH, and RO<sub>2</sub> for the four lighting conditions. The abrupt concentration changes at 10:00 h and noon are caused by the ventilation system switching off and on, respectively. The OH concentration is ~3 × 10<sup>5</sup> molecule/cm<sup>3</sup> under no lighting

or lighting by covered or bare fluorescent tubes, and ~5 × 10<sup>5</sup> molecule/cm<sup>3</sup> with attenuated outdoor light before the emission starts. This enhancement is caused by production through Reaction 7, since NO concentrations are ~2× higher under attenuated outdoor light before ventilation is turned off than the other conditions (not shown) due to enhanced NO<sub>2</sub> photolysis:



The OH concentration decreases once the ventilation is turned off under all conditions and recovers once ventilation is turned on again. With ventilation, O<sub>3</sub> and VOC concentrations are replenished indoors permitting reactive chemistry to occur and OH radicals to form. The concentrations of HO<sub>2</sub> are similar for the first three lighting conditions before the ventilation is turned off and after it is turned back on again. For attenuated outdoor light, the HO<sub>2</sub> and RO<sub>2</sub> concentrations are lower before the ventilation is turned off owing to suppression by NO (eg, Reaction 7 for HO<sub>2</sub>). The main HO<sub>2</sub> source under these conditions is reactions with OH, so the two radicals display similar behavior, with the HO<sub>2</sub> concentration decreasing with OH when ventilation is turned off. When ventilation is turned off, RO<sub>2</sub> concentration rapidly increases and then decays. This is due to OH reacting quickly with any remaining VOCs to form RO<sub>2</sub> radicals, which then react with any NO present. As NO concentrations are lower in the dark (not shown), peak RO<sub>2</sub> is highest under these conditions. After ventilation resumes, RO<sub>2</sub> levels return to the initial values.

#### 3.2 | Disinfectant gases

Figure 4 shows the predicted temporal profiles of the four disinfectant gases under the different lighting conditions. The profiles for each disinfectant (except OCIO) are very similar: A rapid increase in concentration during fumigation, peaking when disinfection stops at around 11:00 h, followed by a decrease to background levels over the course of ~1.5 hours after generation ceases. Peak concentrations are similar for different lighting conditions.

As shown in Figure 2, OCIO absorbs light much more strongly than the other disinfectant gases at wavelengths present indoors. The temporal profile of its concentration is therefore greatly affected by the illumination conditions. Peak OCIO concentrations are greatest in the dark; under attenuated sunlight, they are

**TABLE 1** Calculated OH production rates from O<sub>3</sub> photolysis by sunlight (ATT), covered (CF), and bare (BF) fluorescent bulbs at a distance of 1 m for peak (25 ppm), 300, 100, and 30 ppb O<sub>3</sub>; INDCM predicted OH concentrations at the same points; and calculated photolysis rate constants 1 m from each light source based on data from Ref. 54

Light Source	Peak O <sub>3</sub> /ppm	Photolysis rate constant/s	Rates in molecule/cm <sup>3</sup> /s and (in parentheses) [OH] in 10 <sup>5</sup> molecule/cm <sup>3</sup>			
			Peak O <sub>3</sub>	300 ppb	100 ppb	30 ppb
Dark	24.9	0	0 (13.4)	0 (3.7)	0 (3.3)	0 (2.7)
CF	24.9	1.29 × 10 <sup>-10</sup>	2.5 × 10 <sup>4</sup> (14.1)	298 (3.7)	99.2 (3.3)	29.8 (2.8)
BF	24.8	1.27 × 10 <sup>-6</sup>	2.4 × 10 <sup>8</sup> (127)	2.9 × 10 <sup>6</sup> (4.3)	9.8 × 10 <sup>5</sup> (3.7)	2.9 × 10 <sup>5</sup> (2.9)
ATT	24.8	2.06 × 10 <sup>-8</sup>	3.9 × 10 <sup>6</sup> (13.9)	4.8 × 10 <sup>4</sup> (3.8)	1.6 × 10 <sup>4</sup> (3.4)	4765 (2.8)

**TABLE 2** Predicted HO<sub>2</sub> production rates from HCHO photolysis by sunlight (ATT), covered (CF), and bare (BF) fluorescent bulbs at a distance of 1 m for peak, 1 ppm and 2.6 ppb HCHO; INDCM predicted HO<sub>2</sub> concentrations at the same points; and calculated photolysis rate constants 1m from each light source based on data from Ref. 54

Light Source	Peak HCHO/ ppm	Photolysis rate constant at 1 m/s	Rates in molecule/cm <sup>3</sup> /s and (in parentheses) [HO <sub>2</sub> ] in ppt		
			Peak HCHO	1 ppm	2.6 ppb
Dark	982	0	0 (6)	0 (12.4)	0 (6.4)
CF	982	0	0 (7.2)	0 (12.8)	0 (6.4)
BF	978	$7.7 \times 10^{-7}$	$3.7 \times 10^{10}$ (2424)	$3.8 \times 10^7$ (69.6)	$9.9 \times 10^4$ (7.2)
ATT	1053	$5.2 \times 10^{-9}$	$2.7 \times 10^8$ (203)	$2.6 \times 10^5$ (14)	$6.7 \times 10^2$ (6.4)

only ~3% that predicted in the dark due to rapid photolysis. This extremely rapid photolysis is the reason OCIO must be prepared and stored in the dark, as noted in the Introduction. The temporal profile for OCIO looks very different than the other gases, particularly in the dark and for attenuated outdoor light. OCIO is only removed in the model through photolysis, or reaction with NO, Cl, O or OH (see Supporting Information). Given the formation of these four species is photolysis-dependent, their reaction rates are relatively slow in the dark. The flat peak between ~11:00-12:00 h occurs because emission has stopped but ventilation is still turned off and there is no effective loss. Once ventilation is resumed, the OCIO is gradually removed. For attenuated outdoor light, there is also a (narrower) flat-topped peak; in this instance, the flat peak is caused by the balance between emission strength and photolysis

rate between 10:00-11:00 h. Once the emission ceases, the remaining OCIO is rapidly photolyzed.

### 3.3 | Ozone

The primary radical generated by O<sub>3</sub> photolysis is OH (Figure 1). Table 1 illustrates predicted OH formation rates at ozone concentrations corresponding to baseline levels in hospitals (30 ppb), during cleaning events (~25 ppm), at the short-term and long-term exposure limits (300 and 100 ppb),<sup>45</sup> as well as steady-state OH concentrations predicted by the model at each O<sub>3</sub> mixing ratio. Photolysis rates are low in the dark and under illumination by covered fluorescents and attenuated sunlight; the rates under these conditions ( $<5 \times 10^6$  molecule/cm<sup>3</sup>/s) are lower

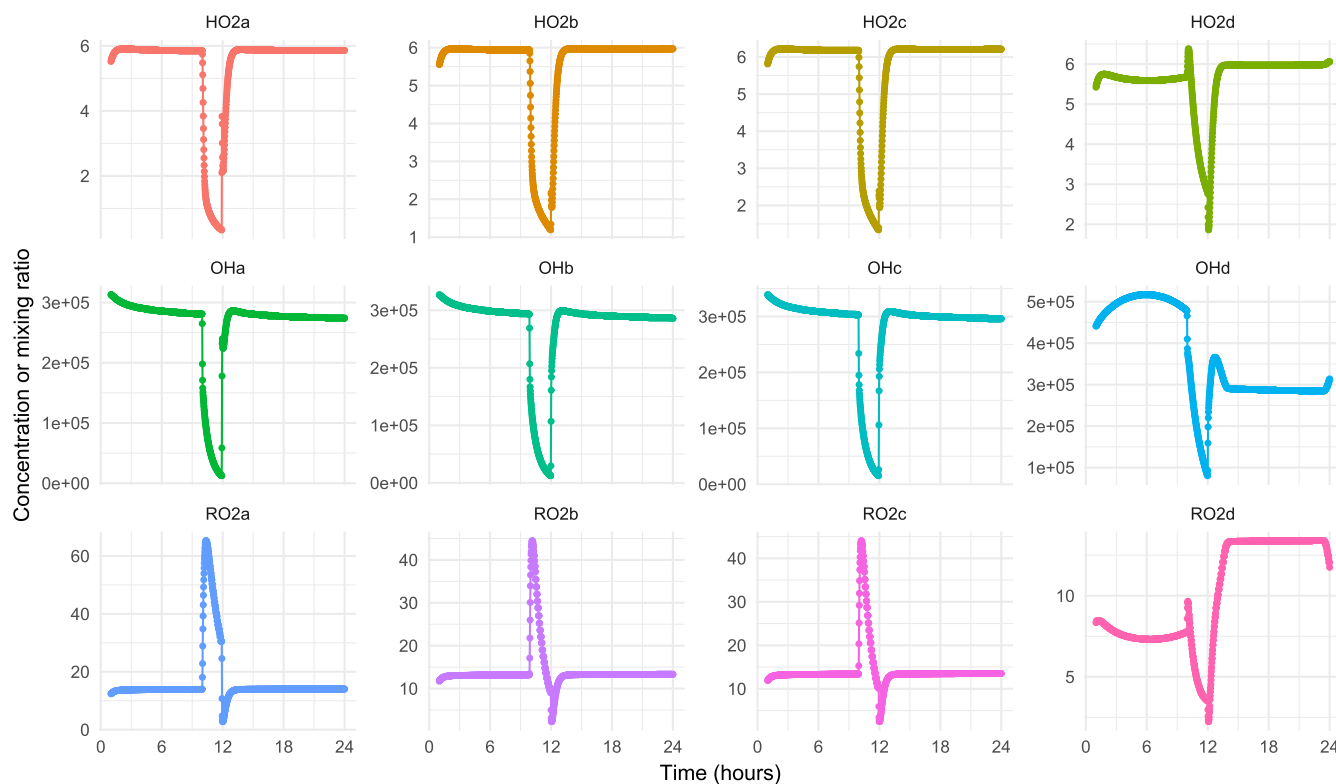


**FIGURE 3** Profiles of baseline (without any fumigant emission) HO<sub>2</sub>, OH, and RO<sub>2</sub> under different lighting conditions (a: dark; b: CF; c: BF; d: ATT) over the course of the study day. Concentrations of HO<sub>2</sub> and RO<sub>2</sub> are in ppt, and concentrations of OH are in molecule/cm<sup>3</sup>. Note that the changes at 10:00 h and noon are driven by the ventilation system being turned off and on, respectively

**TABLE 3** Predicted OH production rates from H<sub>2</sub>O<sub>2</sub> photolysis by sunlight (ATT), covered (CF), and bare (BF) fluorescent bulbs at a distance of 1 m for peak, 120, 1, and 0.001 ppm H<sub>2</sub>O<sub>2</sub>; INDCM predicted OH concentrations at the same points; and calculated photolysis rate constants 1 m from each light source based on data from Ref. 54

Light Source	Peak H <sub>2</sub> O <sub>2</sub> /ppm	Photolysis rate constant/s	Rates in molecule/cm <sup>3</sup> /s and (in parentheses) [OH] in 10 <sup>5</sup> molecule/cm <sup>3</sup>			
			Peak H <sub>2</sub> O <sub>2</sub>	120 ppm	1 ppm	1 ppb
Dark	495	0	0 (0.0003)	0 (0.0004)	0 (1.4)	0 (2.8)
CF	495	9.5 × 10 <sup>-10</sup>	2.3 × 10 <sup>7</sup> (0.01)	5.7 × 10 <sup>6</sup> (0.01)	4.7 × 10 <sup>4</sup> (1.5)	47.3 (3.0)
BF	494	1.6 × 10 <sup>-7</sup>	3.9 × 10 <sup>9</sup> (1.9)	9.4 × 10 <sup>8</sup> (1.9)	7.8 × 10 <sup>6</sup> (3.5)	7800 (3.0)
ATT	524	1.2 × 10 <sup>-7</sup>	3.2 × 10 <sup>9</sup> (1.5)	7.4 × 10 <sup>8</sup> (1.5)	6.2 × 10 <sup>6</sup> (3.5)	6150 (3.0)

than those calculated for ozonation of alkenes in the dark under common indoor conditions of  $\sim 1 \times 10^7$  molecule/cm<sup>3</sup>/s.<sup>49</sup> Photolysis under these illumination conditions is negligible due to very small O<sub>3</sub> photolysis quantum yields at wavelengths longer than 320 nm (Figure 1). Correspondingly, OH concentrations under illumination from covered fluorescents and attenuated sunlight are similar to those in the dark. The photolysis rate under illumination from bare fluorescent tubes is 2 orders of magnitude higher than that from sunlight because bare fluorescent tubes emit light at  $\sim 312$  nm, where the O<sub>3</sub> photolysis quantum yield is much higher than at longer wavelengths. This photolysis results in very high peak OH steady-state concentrations ( $1.3 \times 10^7$  molecule/cm<sup>3</sup>). For context, outdoor OH concentrations in unpolluted urban centers are generally a few  $\times 10^6$  molecule/cm<sup>3</sup>.<sup>79</sup>

Figure 5 shows predicted time-resolved profiles of the radical species. Peak values of OH, HO<sub>2</sub>, and RO<sub>2</sub> with O<sub>3</sub> emission are similar for the dark, covered fluorescent bulb, and attenuated sunlight

conditions. Both OH and HO<sub>2</sub> are  $\sim 2\times$  higher for the bare fluorescent tube, whereas RO<sub>2</sub> concentrations are similar under all conditions. In the dark, under covered fluorescent lighting and attenuated sunlight, OH, HO<sub>2</sub>, and RO<sub>2</sub> concentrations peak when the ventilation is turned off at 10:00 h, as O<sub>3</sub> reacts with VOCs to form OH (and HO<sub>2</sub> and RO<sub>2</sub>). However, given the short radical lifetimes, radical concentrations decrease rapidly once the VOCs are titrated. There is additional HO<sub>2</sub> loss due to reaction with O<sub>3</sub>; OH levels are too low to regenerate HO<sub>2</sub> except under BF conditions, when OH is formed rapidly via O<sub>3</sub> photolysis. A second spike in OH and HO<sub>2</sub> concentrations (under all conditions except BF) is observed just after noon when the ventilation is turned back on and VOCs are re-introduced indoors. Radicals are formed from VOCs reacting with O<sub>3</sub> at this time. This production of radicals is more sustained for RO<sub>2</sub> than for OH or HO<sub>2</sub>, due to relatively high O<sub>3</sub> concentration under these conditions (still at  $\sim 0.8$  ppm at 12:40 h). This O<sub>3</sub> removes the NO that

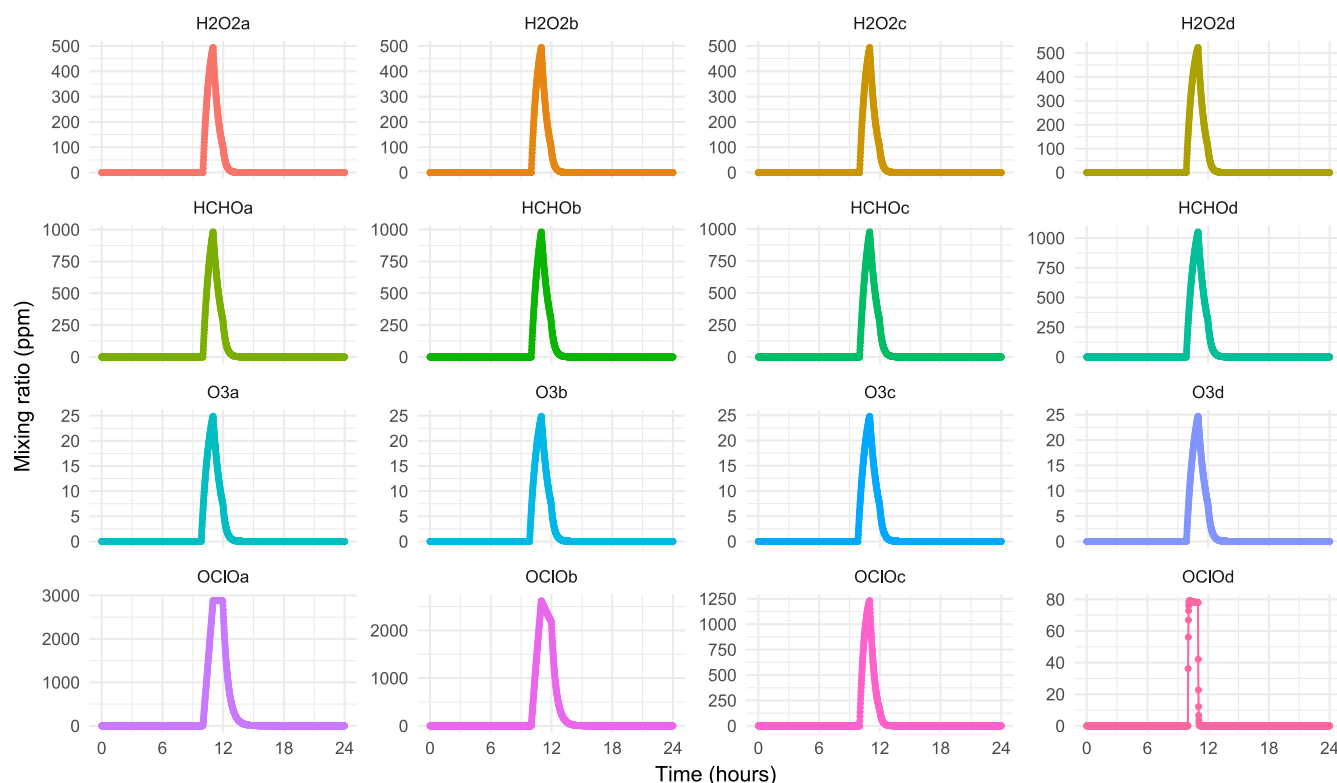
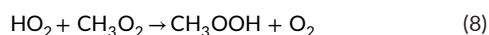


**FIGURE 4** O<sub>3</sub>, HCHO, H<sub>2</sub>O<sub>2</sub>, and OCIO concentrations under different lighting conditions (a: dark; b: CF; c: BF; d: ATT) over the course of the study day



would otherwise suppress RO<sub>2</sub> concentrations. The RO<sub>2</sub> only begins to decrease once the NO recovers at around 13:00 h.

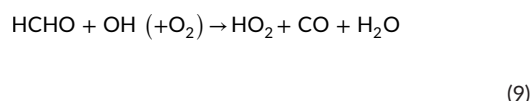
For bare fluorescent bulb lighting OH and HO<sub>2</sub> radicals show a single peak that coincides temporally with peak O<sub>3</sub> concentrations at 11:00 h. Peak concentrations are much higher than under the weaker illumination conditions, owing to the much higher O<sub>3</sub> photolysis rates under these conditions (Table 1). The behavior of RO<sub>2</sub> under BF is similar to that under the other lighting conditions. The higher HO<sub>2</sub> concentrations under BF conditions also suppress RO<sub>2</sub> through reactions such as Reaction 8:



### 3.4 | Formaldehyde

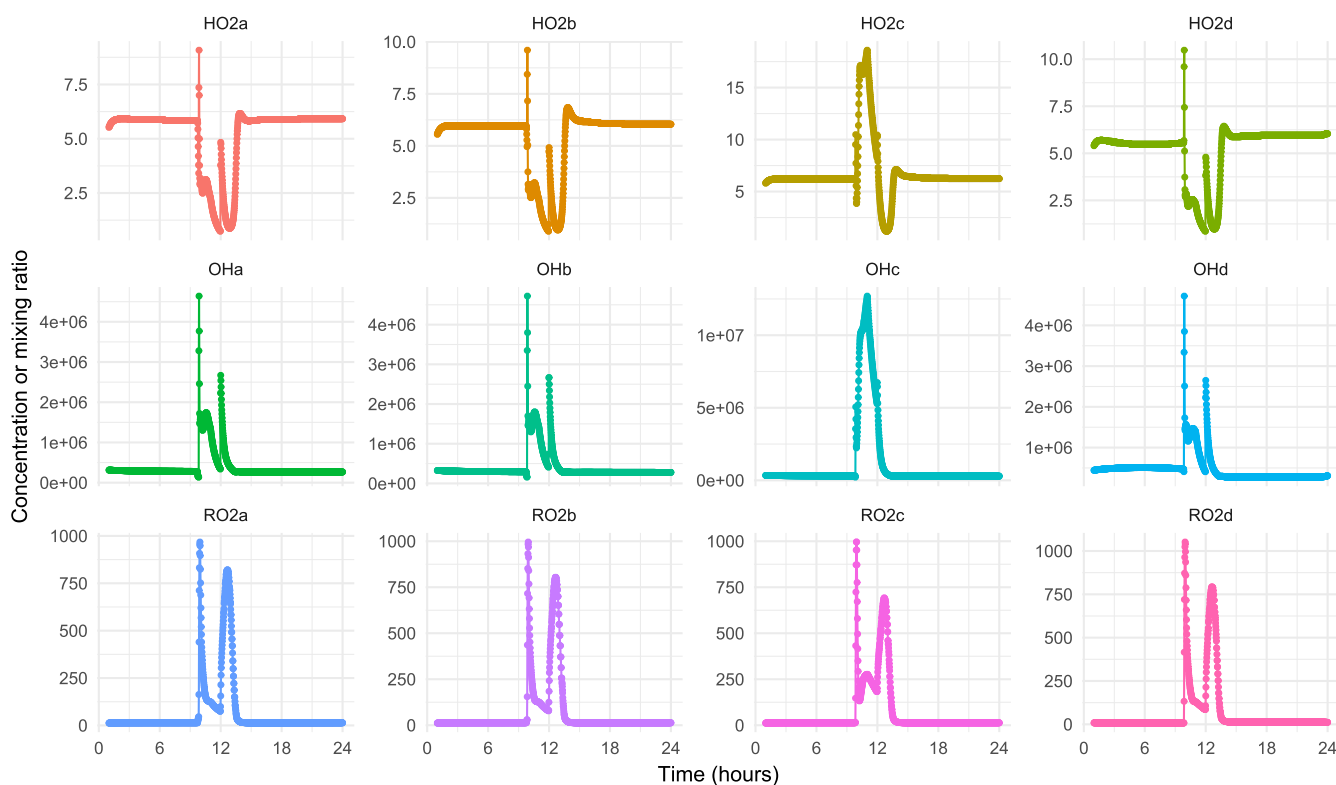
Table 2 reports predicted HO<sub>2</sub> production rates for various lighting conditions for formaldehyde levels corresponding to the baseline level used in the model (2.6 ppb), during cleaning events (~1000 ppm), and at the long-term exposure limit (1 ppm).<sup>44</sup> The HO<sub>2</sub> radicals are produced following HCHO photolysis (Figure 1). At peak HCHO levels generated during cleaning events, the model predicts a steady-state HO<sub>2</sub> concentration of ~2.4 ppb under illumination from a bare fluorescent tube. Predicted concentrations remain elevated even after HCHO levels decrease below the long-term exposure limits (when people are allowed back into the room) especially under illumination by bare fluorescent bulbs, with concentrations of ~70 ppt at 1 ppm HCHO.

Figure 6 shows the time-resolved model predictions of radical concentrations following HCHO fumigation. Peak concentrations of HO<sub>2</sub> correlate with photolysis rate (Table 2) given the direct formation through HCHO photolysis. Hydroperoxy radicals produced from formaldehyde photolysis have three major fates: react with each other to form hydrogen peroxide, with RO<sub>2</sub> to form organic peroxides, or with nitric oxide to form hydroxyl radicals. For peak HCHO concentration, the self-reaction dominates HO<sub>2</sub> loss for bare fluorescent or attenuated outdoor lighting, while for the other two conditions, reaction with RO<sub>2</sub> is most important. For the other HCHO concentrations shown in Table 2, reaction with NO dominates HO<sub>2</sub> loss under all lighting conditions. Note that HO<sub>2</sub> is formed directly from HCHO photolysis, but also from Reaction 9:



This means that even when the photolysis rate of HCHO to form HO<sub>2</sub> is negligible (under no/low lighting conditions), it is still possible to form HO<sub>2</sub>, though at lower concentrations than observed under illumination from fluorescent tubes or attenuated sunlight.

Although OH is formed from the reaction between HO<sub>2</sub> and NO, its concentration depends negatively on HCHO concentrations. This is because HCHO is an OH sink (via Reaction 9), and loss of OH to HCHO is greater than formation from HO<sub>2</sub> and NO. Thus, OH levels during and immediately after disinfection are lower than under background conditions for all lighting conditions. The OH and RO<sub>2</sub>



**FIGURE 5** Profiles of HO<sub>2</sub>, OH, and RO<sub>2</sub> under different lighting conditions (a: dark; b: CF; c: BF; d: ATT) for O<sub>3</sub> emission. Concentrations of HO<sub>2</sub> and RO<sub>2</sub> are in ppt, and concentrations of OH are in molecule/cm<sup>3</sup>

**TABLE 4** Predicted Cl production rates from OClO photolysis by sunlight (ATT), covered (CF), and bare (BF) fluorescent bulbs at a distance of 1 m for peak, 300, 100, and 10 ppb OClO; INDCM predicted Cl concentrations at the same points; and calculated photolysis rate constants 1 m from each light source based on data from Ref. 54

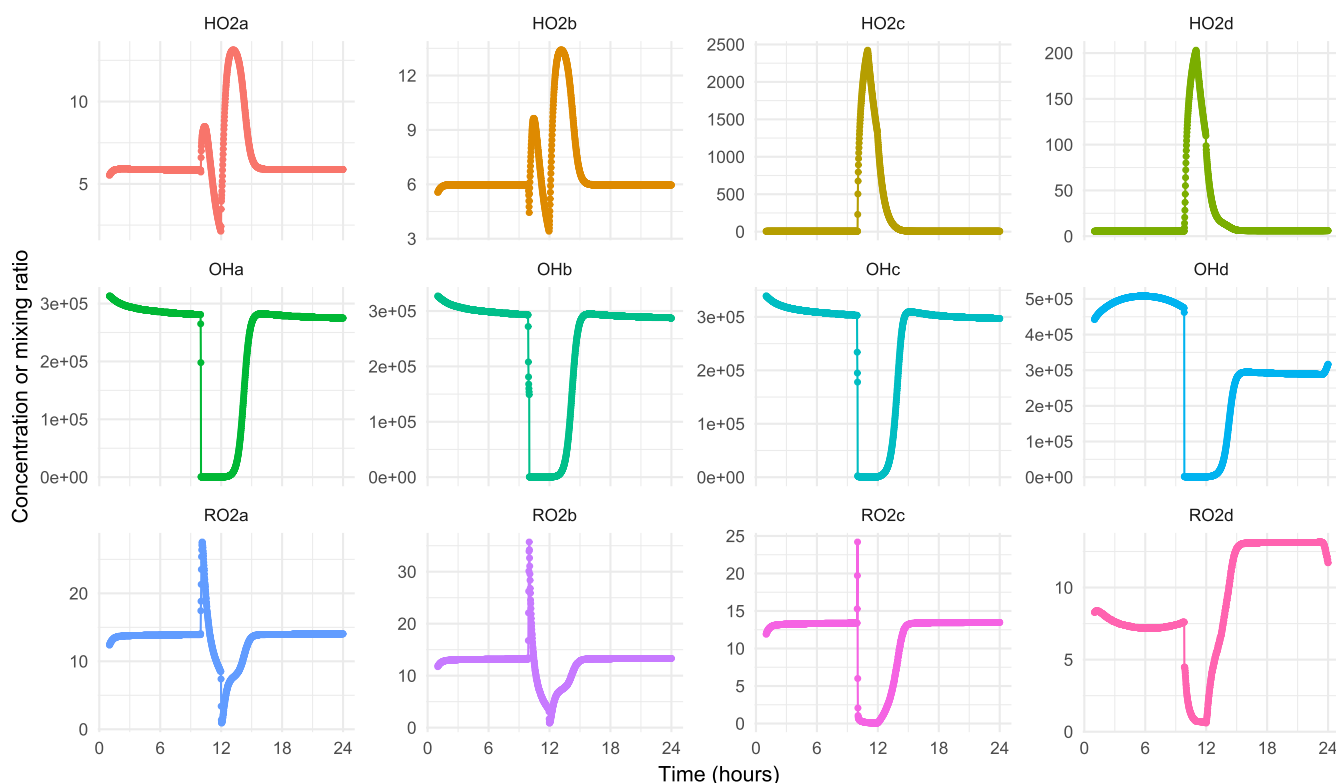
Light Source	Peak OClO/ ppm	Photolysis rate constant/s	Rates in molecule/cm <sup>3</sup> /s and (in parentheses) [Cl] in 10 <sup>5</sup> molecule/cm <sup>3</sup>			
			Peak OClO	300 ppb	100 ppb	10 ppb
Dark	2879	0	0 (0)	0 (1 × 10 <sup>-5</sup> )	0 (6 × 10 <sup>-5</sup> )	0 (6 × 10 <sup>-4</sup> )
CF	2623	4.9 × 10 <sup>-5</sup>	3.9 × 10 <sup>11</sup> (0.003)	3.7 × 10 <sup>8</sup> (0.6)	1.2 × 10 <sup>8</sup> (1.1)	1.2 × 10 <sup>7</sup> (0.02)
BF	1232	5.3 × 10 <sup>-4</sup>	2.0 × 10 <sup>12</sup> (2.8)	4.0 × 10 <sup>9</sup> (26.4)	1.3 × 10 <sup>9</sup> (27.9)	1.3 × 10 <sup>8</sup> (24.3)
ATT	79	9.9 × 10 <sup>-3</sup>	2.4 × 10 <sup>12</sup> (27.7)	7.4 × 10 <sup>10</sup> (75.4)	2.5 × 10 <sup>10</sup> (76.8)	2.5 × 10 <sup>9</sup> (79.6)

concentrations for attenuated outdoor light are also notably higher and lower respectively before the emission than afterward. This is because of elevated NO under these lighting conditions compared to the others (see Section 3.1). RO<sub>2</sub> concentrations are also suppressed by the high concentrations of HO<sub>2</sub> when HCHO is the disinfectant gas (eg, Reaction 8).

For all conditions, there is a brief peak in RO<sub>2</sub> concentrations at 10:00 h as OH reacts with the remaining VOCs to form RO<sub>2</sub>, and then a decrease as HO<sub>2</sub> concentrations increase and react with RO<sub>2</sub> (eg, via Reaction 8). The concentration of RO<sub>2</sub> then increases again after 12:00 h as ventilation resumes and oxidation reactions restart. There is a sharp increase and peak of NO at 12:00 h under dark and covered fluorescent lighting conditions (not shown) when the ventilation is turned back on which causes the RO<sub>2</sub> concentration to decrease sharply to a very low concentration.

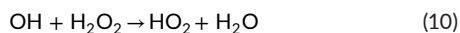
### 3.5 | Hydrogen peroxide

Table 3 illustrates predicted OH production rates at H<sub>2</sub>O<sub>2</sub> concentrations during cleaning events (~500 and 120 ppm), at the long-term exposure limit (1 ppm),<sup>43</sup> and at background levels (1 ppb).<sup>80</sup> Hydroxyl radical formation rates are high at peak H<sub>2</sub>O<sub>2</sub> levels during disinfection under illuminated conditions (~2 × 10<sup>7</sup> molecules/cm<sup>3</sup>/s for covered fluorescent tubing and 3–4 × 10<sup>9</sup> molecules/cm<sup>3</sup>/s for bare fluorescent and attenuated outdoor light). Formation rates remain significant (ie, on the same order of magnitude as formation via ozone-alkene reactions) even at 1 ppm H<sub>2</sub>O<sub>2</sub> under stronger lighting conditions (BF and ATT). Despite rapid formation, OH steady-state concentrations are similar to or lower than those under baseline conditions at all H<sub>2</sub>O<sub>2</sub> concentrations. This is because OH is removed by H<sub>2</sub>O<sub>2</sub> via Reaction 10 at a greater rate (more than 100× faster for attenuated outdoor



**FIGURE 6** Profiles of HO<sub>2</sub>, OH, and RO<sub>2</sub> under different lighting conditions (a: dark; b: CF; c: BF; d: ATT) for HCHO emission. Concentrations of HO<sub>2</sub> and RO<sub>2</sub> are in ppt, and concentrations of OH are in molecule/cm<sup>3</sup>

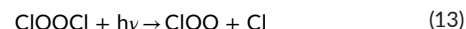
and bare fluorescent lighting) than it is produced from photolysis (via Equation 4).



The temporal profiles of OH (Figure 7) resemble those under baseline conditions, although the minima last longer due to loss of OH through Reaction 10. In the dark and with covered fluorescent lighting, OH concentrations are well below baseline levels (of  $3 \times 10^5$  molecule/cm) when  $\text{H}_2\text{O}_2$  levels are elevated and are close to baseline levels when  $\text{H}_2\text{O}_2$  decreases to  $< 1$  ppm. Under bare fluorescent and attenuated sunlight conditions, OH concentrations increase somewhat compared to the darker conditions, for similar reasons as for the HCHO simulation. Unlike OH, the temporal profiles of  $\text{HO}_2$  do not resemble background conditions. Small fluctuations in  $\text{HO}_2$  concentrations are observed during disinfection in the dark, but clear increases are observed under illumination by all light sources, with much higher concentrations observed under bare fluorescent and attenuated outdoor light than covered fluorescent light. The elevated  $\text{HO}_2$  levels are from Reaction 10, and time-dependent  $\text{HO}_2$  concentrations under illuminated conditions correlate with  $\text{H}_2\text{O}_2$  concentrations. The trends for  $\text{RO}_2$  during  $\text{H}_2\text{O}_2$  fumigation are similar to those for HCHO fumigation. Once high concentrations of  $\text{HO}_2$  are formed via Reaction 10, reactions between  $\text{HO}_2$  and  $\text{RO}_2$  to form peroxides (eg, Reaction 8) suppress  $\text{RO}_2$ .

### 3.6 | Chlorine dioxide

Chlorine dioxide photolysis forms oxygen atoms and ClO radicals (Reaction 11). The ClO radical absorption spectrum has little overlap with wavelengths present indoors, except for high-energy photons from bare fluorescent tubes that can form Cl (Reaction 12). ClO dimers can absorb at wavelengths  $> 500$  nm. Under NTD cleaning conditions, there is likely sufficient production of ClO to form dimers, which photolyze to form chloroperoxy radicals (ClOO) and Cl (Reaction 13).



There is no ClOO absorbance at wavelengths longer than 280 nm, so there is no overlap with light indoors. Using the steady-state approximation and ignoring other reactions involving reactive intermediates (including photolysis of ClO), the Cl formation rate from ClOO photolysis can be approximated as the rate of ClOO photolysis (Equation 6).

Table 4 reports predicted Cl formation rates at ClOO concentrations corresponding to peak levels ( $\sim 3000$  ppm) during cleaning events, at the short- and long-term exposure limits (300 and 100 ppb,

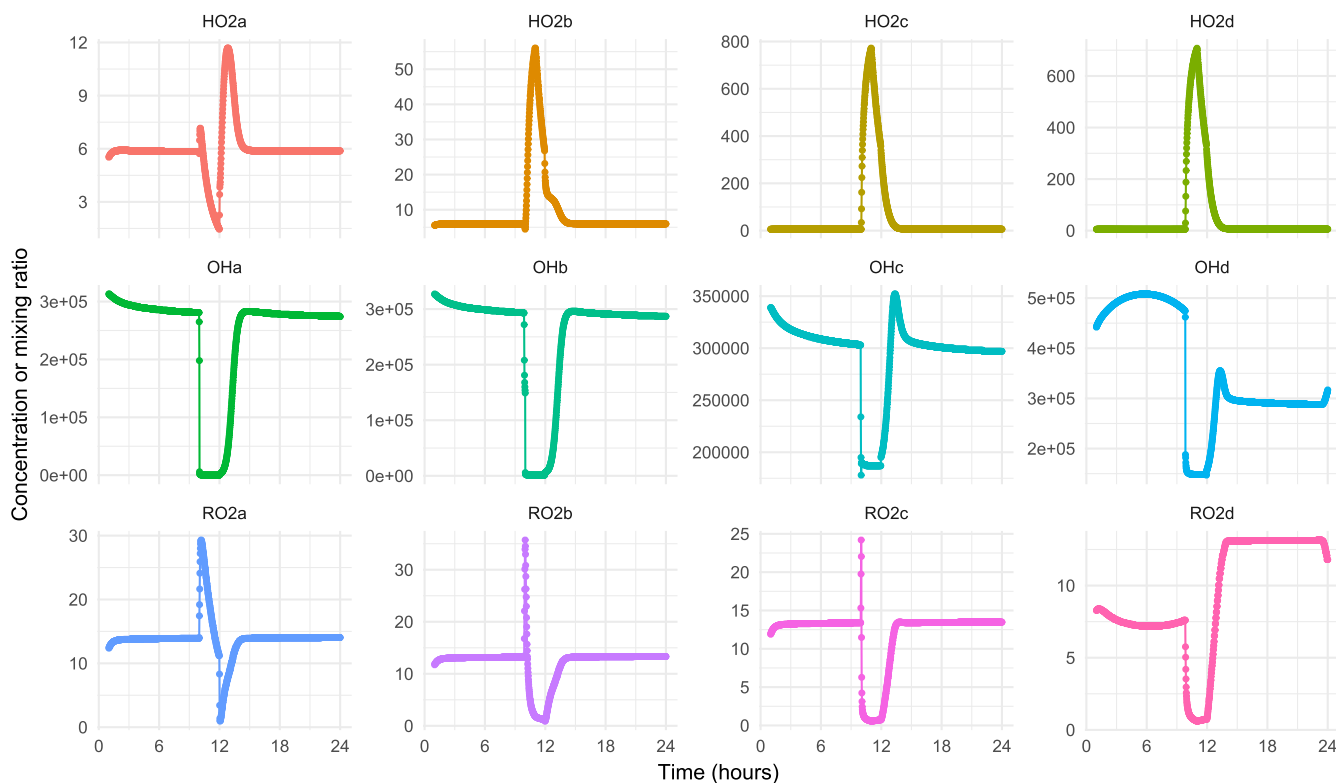


**FIGURE 7** Profiles of  $\text{HO}_2$ , OH, and  $\text{RO}_2$  under different lighting conditions (a: dark; b: CF; c: BF; d: ATT) for  $\text{H}_2\text{O}_2$  emission. Concentrations of  $\text{HO}_2$  and  $\text{RO}_2$  are in ppt, and concentrations of OH are in molecule/cm<sup>3</sup>

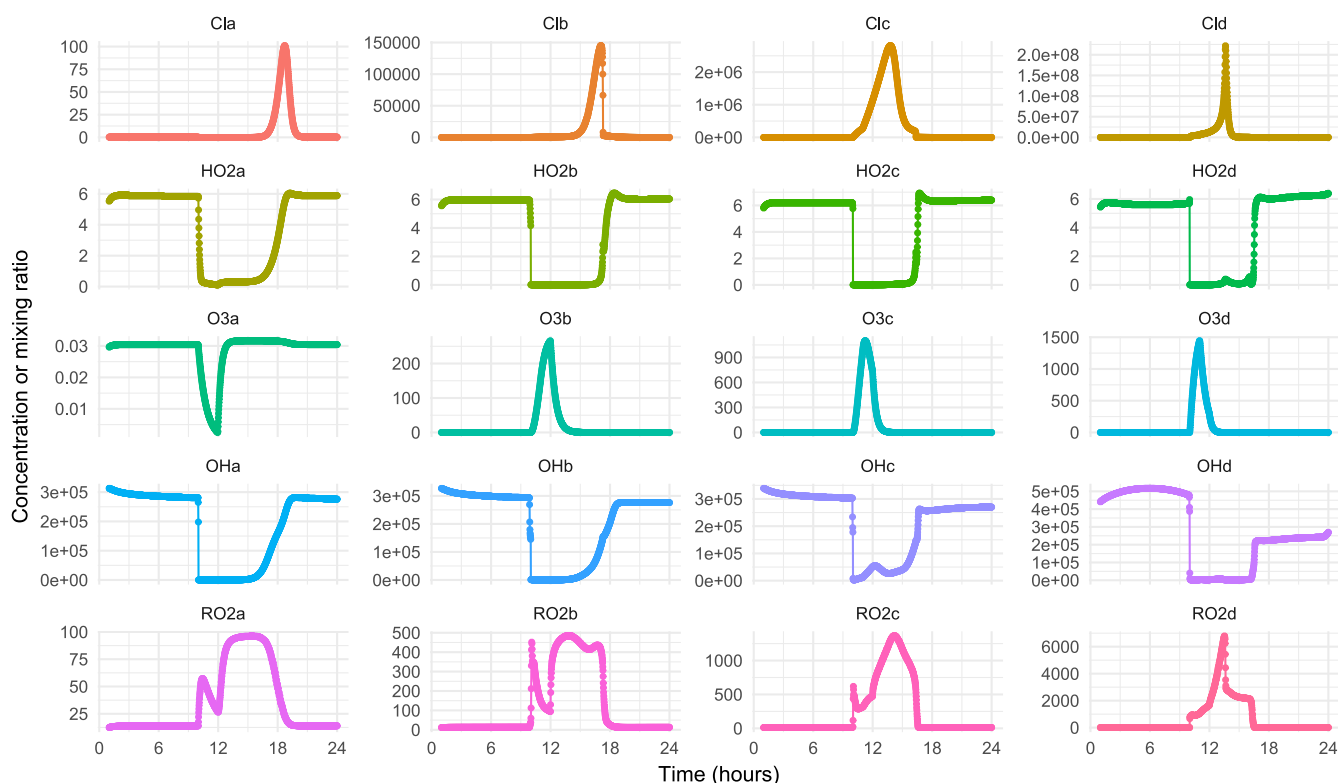
respectively)<sup>45</sup> and at 10 ppb. High Cl formation rates are predicted under illuminated conditions even at 10 ppb OCIO. Steady-state Cl concentrations are elevated at all OCIO concentrations under bare fluorescent and attenuated outdoor lighting, with little dependence on OCIO concentration, despite Cl formation rates that decrease by 4 or 5 orders of magnitude between peak OCIO concentrations and 10 ppb. This is because species involved in the reactions that lead to Cl formation, as well as Cl itself, can undergo competing reactions (Figure 1), some of which depend on light and OCIO concentrations. This chemistry can be understood by examining the time-resolved concentrations of relevant species (Cl, HO<sub>2</sub>, OH, RO<sub>2</sub> and O<sub>3</sub>), shown in Figure 8.

Figure 4 showed that the time-dependent behavior of OCIO is very different from the other disinfectant gases studied. This is because it is extremely photolabile, even at wavelengths relevant to indoor environments (Figure 2). The temporal profiles of radicals and other oxidants formed during OCIO disinfection are also very different than those produced from other disinfectant gases. Small amounts of Cl are formed in the dark, and very high peak levels are observed under illuminated conditions ( $1.5 \times 10^5$ ,  $2.8 \times 10^6$ , and  $2.2 \times 10^8$  molecule/cm<sup>3</sup> for covered and bare fluorescent and attenuated outdoor lighting respectively). Note that peak Cl concentrations do not coincide temporally with peak OCIO concentrations. For instance, peak Cl levels are observed 167 minutes after OCIO levels peak with bare fluorescent lighting, and 208 minutes after OCIO levels peak in attenuated outdoor light. Peak OCIO concentrations are always at around 11:00 h (except for ATT where they occur just after 10:00 h), whereas the peak in ozone gets earlier as

the OCIO photolysis rate increases, occurring at 11:00 h for ATT, but after 15:00 h in the dark. Given that Cl reacts rapidly with O<sub>3</sub>, Cl concentrations only peak once O<sub>3</sub> concentrations have decreased.

Concentrations of OH and HO<sub>2</sub> decrease at around 10:00 h, returning to “normal” with a slower recovery rate compared to OH trends for the emission of other gases. When ClO concentrations are high in the more intense light conditions, OH and HO<sub>2</sub> react with ClO and are depleted. In the dark, OH reacts with OCIO, only returning to background concentrations when OCIO is no longer present. An increase in RO<sub>2</sub> levels is observed under all illumination conditions, with the highest levels observed under ATT. In the dark, RO<sub>2</sub> is formed as the remaining VOCs react with OH when the ventilation is turned off. Under the illuminated conditions, the Cl produced by photolysis can additionally oxidize VOCs to form RO<sub>2</sub>. The RO<sub>2</sub> concentration is therefore enhanced relative to the dark case, particularly for bare fluorescent and attenuated sunlight conditions. Moreover, as shown in Table 4, OCIO photolysis under attenuated sunlight is ~20 times faster than under bare fluorescent lighting, resulting in an earlier (~40 minutes) and higher peak of RO<sub>2</sub>. Once the ventilation is turned back on, the chlorine radicals are slowly depleted, which means the opportunities to form more RO<sub>2</sub> become limited and the RO<sub>2</sub> eventually decreases.

The confounding factor with using OCIO as a disinfectant gas is that photolysis of OCIO produces O atoms (Reaction 11), which react with O<sub>2</sub> to produce O<sub>3</sub>. Depending on the light levels, this can produce high ozone levels (with peak concentrations of 1100 ppm for BF and 1440 ppm for ATT, as shown in Figure 8) that can then



**FIGURE 8** Profiles of Cl, HO<sub>2</sub>, O<sub>3</sub>, OH, and RO<sub>2</sub> under different lighting conditions (a: dark; b: CF; c: BF; d: ATT) for OCIO emission. Concentrations of HO<sub>2</sub> and RO<sub>2</sub> are in ppt, concentrations of Cl and OH are in molecule/cm<sup>3</sup>, and concentrations of O<sub>3</sub> are in ppm.

affect the chemistry. We note that the  $O_3$  levels generated from OCIO photolysis are much higher than those commonly attained using  $O_3$  as the primary fumigant (25 ppm). The combination of high OCIO and  $O_3$  concentrations means that OH is suppressed for many hours following disinfection. Although OH radicals can be produced via  $O_3$  photolysis, the reaction of  $O_3$  with Cl is a more important loss route for  $O_3$ , particularly under attenuated sunlight conditions. Any OH that forms therefore rapidly reacts with the OCIO that is formed through the reaction of Cl with  $O_3$ .

We also ran the model assuming peak OCIO concentrations of 350 ppm as per the Introduction. We found that under these conditions, Cl concentrations peaked in the attenuated sunlight conditions at  $\sim 2 \times 10^7$  molecule/cm<sup>3</sup>. These values reflect the fact that the OCIO emission into the room is  $\sim 10$  times lower than under the conditions illustrated in Figure 8.

## 4 | IMPLICATIONS

We have predicted indoor OH, HO<sub>2</sub>, RO<sub>2</sub>, and Cl production rates and concentrations during and after NTD cleaning events. Our results suggest that concentrations of these radicals during cleaning events may be orders of magnitude higher than indoor and outdoor baseline levels and that elevated concentrations may persist for several hours after the cleaning event. Long-term exposure limits (when rooms are deemed safe for reentry) are reached 2-4.5 hours after disinfection ceases, depending on the disinfectant gas used and the illumination condition. Table 5 shows radical concentrations when rooms are considered safe for reentry for each disinfectant gas under different lighting conditions. It is clear that these can remain elevated under some conditions many hours after disinfection, especially for the bare fluorescent and attenuated sunlight conditions. Note also that when OCIO is used as a disinfectant gas,  $O_3$  levels can also remain elevated after OCIO concentrations reach a safe limit: under bare fluorescent lighting,  $O_3$  concentrations are still 3.5 ppm and for attenuated outdoor light, 1150 ppm, well above the safe limit for  $O_3$  of 100 ppb. We also considered exposure to the total radical concentrations (OH + HO<sub>2</sub> + RO<sub>2</sub> + Cl) over the 24 h of the cleaning day (see Table S3). The biggest exposure to total radical concentration is for OCIO (ATT) at  $\sim 1$  ppm with the second biggest exposure to radicals of  $\sim 0.3$  ppm for HCHO (BF).

**TABLE 5** Concentrations of OH (yellow), HO<sub>2</sub> (pink), Cl (green) (OCIO only), and RO<sub>2</sub> (cyan), clockwise from top left for the 4 disinfectant gases at the time when the disinfectant gas has returned to the long-term exposure limit value. OH and Cl concentrations in 10<sup>5</sup> molecule/cm<sup>3</sup>. HO<sub>2</sub> and RO<sub>2</sub> concentrations in ppt

	$O_3$		HCHO		H <sub>2</sub> O <sub>2</sub>		OCIO	
dark	3.2	1.1	0.4	12.5	1.4	10.3	0.8	1.1
	418.4	/	8.5	/	10.2	/	85.1	0.0
CF	3.3	1.2	0.5	12.8	1.5	10.5	0.7	0.1
	430.4	/	8.0	/	9.8	/	432.8	1.1
BF	3.7	1.4	1.1	69.4	3.5	24.3	0.3	0.0
	399.5	/	6.3	/	11.9	/	1259.4	27.9
ATT	3.4	1.3	0.5	13.9	3.5	21.5	0.0	0.0
	367.8	/	7.7	/	10.5	/	1192.8	76.8

Background levels of the radicals studied in this work (when ventilation is running) are as follows:  $3-5 \times 10^5$  molecules/cm<sup>3</sup> (OH), 6 ppt (HO<sub>2</sub>), 0 molecule/cm<sup>3</sup> (Cl), and 8-15 ppt (RO<sub>2</sub>). For cleaning events, after  $O_3$  concentrations have decreased to safe levels, OH, HO<sub>2</sub>, and Cl will be at or near baseline levels, but Table 5 shows that RO<sub>2</sub> will be greatly elevated ( $\sim 400$  ppt under all conditions). After HCHO has reached safe levels, HO<sub>2</sub> will be greatly elevated under illumination by bare fluorescent bulbs ( $\sim 70$  ppt). After H<sub>2</sub>O<sub>2</sub> levels have decreased to safe levels, HO<sub>2</sub> will be elevated by 3-4 times compared to background levels under illumination from bare fluorescent tubes and attenuated sunlight. After OCIO has returned to safe levels, Cl will be elevated under these same two lighting conditions ( $2.8 \times 10^6$  and  $7.7 \times 10^6$  molecule/cm<sup>3</sup> respectively), and RO<sub>2</sub> will be elevated under all conditions, ranging from 85 ppt in the dark to  $\sim 1.2$  ppb under illumination by bare fluorescent tubes and attenuated outdoor light. These elevated concentrations could lead to the formation of harmful secondary pollutants such as chlorinated and oxygenated organics and particulate matter, resulting in a temporary but significant decrease in air quality in rooms employing NTDs. Note that there are also likely to be significant surface interactions for some of the fumigants, which will likely lead to additional oxygenated VOCs indoors.<sup>60</sup> Current safety guidelines do not account for potentially elevated radical concentrations either before or after safe levels of the respective compounds are reached. The results of this study in no way suggest that the fumigants discussed should not be used to disinfect hospital rooms; their efficacy at deactivating bacteria makes them an extremely important tool to keep hospitals safe for staff and patients. It is possible, however, that revised operating procedures should be considered for some of these instruments to reduce exposure to photochemically-generated gas-phase species, such as running the instruments in the dark, waiting until ambient levels of the fumigant are an order of magnitude below current safety guidelines, or increasing air change rates during NTD use.

It is important to note that photon fluxes (and therefore radical concentrations) depend on a number of factors. Some factors affecting photon fluxes from fluorescent tubes include brand, color temperature, wattage, age of tube, and number of tubes. Photon fluxes from sunlight depend on numerous factors including time of day, cloud cover, and type of window glass. Photon fluxes will vary greatly throughout a room due to decreases in irradiance with distance, the orientation of windows with respect to the sun, and the presence of objects within the room that block light. In order to accurately predict average radical concentrations within a room ("room-averaged concentrations"), all of these factors would ideally be taken into account.

Room-averaged radical concentrations will vary over the course of the day and will be different from room to room. Rather than estimating volume-averaged radical concentrations for the specific room used in the model at a specific time of day, we consider the radical concentrations we predict using measured photon fluxes from sunlight inside a window and from fluorescent tubes at a distance of 1 m from the tubes to be an adequate approximation of

volume-averaged radical concentrations within a well-lit room. Near noon, irradiance from sunlight has only a weak distance dependence indoors, and photon fluxes are expected to be relatively uniform within illuminated regions.<sup>54</sup> The distance dependence of irradiance from a single fluorescent tube has been reported to follow  $d^{-0.8}$ , where  $d$  is distance from the lamp.<sup>54</sup> The dependence is fairly weak at distances greater than ~25 cm, with only a ~75% decrease between distances of 0.25 m and 1 m from the lamp, and another ~75% decrease between 1 and 2 m from the lamp. This suggests both that calculations performed at a distance of 1 m from the lamp are a good estimate of room-averaged radical levels, and that the distance dependence will introduce relatively small uncertainties compared to uncertainties in model assumptions around deposition rates, surface interactions and the concentrations of disinfectant gases assumed etc. To further investigate the importance of the distance dependence, we performed model runs using photon fluxes from a distance of 25 cm from the lamp as a sensitivity test (SI, Table S4). Under BF conditions, OH and HO<sub>2</sub> concentrations increased by a factor of up to 2-3 at 25 cm compared to 1 m. The RO<sub>2</sub> concentrations tended to be slightly smaller closer to the light source, except for OCIO where they were more than 7 times higher. Cl concentrations were most sensitive to changes in distance from the light source. The sensitivity results show that changes in irradiance of ~3× generally result in increases in radical concentrations of 2-3×. This supports our previous statement that the uncertainty introduced by the distance dependence of irradiance from fluorescent tubes will be smaller than that from other model assumptions. The exception to this is Cl generated from OCIO photolysis, which increased by a factor of 1880 at 25 cm compared to 1 m. When considering room-averaged concentrations, the higher radical levels at 25 cm (compared to 1 m), will likely be offset by lower radical levels at greater distances. Our reported radical levels at 1 m are therefore likely a reasonable representation of room-averaged concentrations.

Significant uncertainties remain regarding radical formation indoors (whether NTDs are employed or not), due primarily to a lack of measurements of indoor radicals and their sources and sinks.<sup>81</sup> The model used in this work has shown good agreement in the past with measured radical concentrations (Carslaw et al),<sup>82</sup> but we have necessarily had to make assumptions around NTD operation and use in the absence of more detailed information. Given these caveats, our study suggests that radical levels may be extremely elevated for extended time periods after NTD use, both in the dark and under common forms of indoor illumination. This work also highlights the need for indoor measurements of species such as OH, HO<sub>2</sub>, Cl, and RO<sub>2</sub> to better predict the effects of NTDs on indoor air quality. As a final note, we suggest that the efficacy of NTDs on reducing loadings of several strains of bacteria should be further studied in the dark and under illumination from different indoor lighting. It is possible that efficacy will be greatly enhanced under common lighting sources such as fluorescent lights due to the production of radicals that may inactivate bacteria more effectively than the disinfection agents. As NTD devices gain popularity, we urge researchers to consider their

potential effects on air quality as well as on bacterial loads, and to determine operating procedures accordingly.

## ACKNOWLEDGEMENTS

This work was supported by funding from the Alfred P. Sloan Foundation (Grants G-2017-9796 for Carslaw and G-2018-11062 for Kahan). Dr Kahan is Canada Research Chair in Environmental Analytical Chemistry. This research was undertaken, in part, thanks to funding from the Canada Research Chairs program.

## AUTHOR CONTRIBUTION

**Zixu Wang:** Data curation (supporting); Formal analysis (lead); Investigation (lead); Methodology (equal); Software (supporting); Validation (equal); Visualization (equal); Writing-original draft (equal); Writing-review & editing (equal). **Shawn F. Kowal:** Conceptualization (equal); Formal analysis (supporting); Investigation (supporting); Methodology (supporting); Validation (supporting); Writing-original draft (equal); Writing-review & editing (supporting). **Nicola Carslaw:** Data curation (lead); Formal analysis (supporting); Funding acquisition (equal); Methodology (equal); Project administration (equal); Resources (lead); Software (lead); Supervision (equal); Validation (equal); Visualization (equal); Writing-original draft (equal); Writing-review & editing (equal). **Tara F. Kahan:** Conceptualization (equal); Formal analysis (supporting); Funding acquisition (equal); Methodology (supporting); Project administration (equal); Resources (supporting); Supervision (equal); Validation (equal); Visualization (equal); Writing-original draft (equal); Writing-review & editing (equal).

## ORCID

Nicola Carslaw  <https://orcid.org/0000-0002-5290-4779>

Tara F. Kahan  <https://orcid.org/0000-0001-5074-1155>

## REFERENCES

1. Boyce JM, Potter-Bynoe G, Chenevert C, King T. Environmental contamination due to methicillin-resistant *Staphylococcus aureus*: Possible infection control implications. *Infect Cont Hosp Epidemiol*. 1997;18(9):622-627.
2. Hardy KJ, Oppenheim BA, Gossain S, Gao F, Hawkey PM. Study of the relationship between environmental contamination with methicillin-resistant *Staphylococcus aureus* (MRSA) and patients' acquisition of MRSA. *Infect Cont Hosp Epidemiol*. 2006;27(2):127-132.
3. Sexton T, Clarke P, O'Neill E, Dillane T, Humphreys H. Environmental reservoirs of methicillin-resistant *Staphylococcus aureus* in isolation rooms: correlation with patient isolates and implications for hospital hygiene. *J Hosp Infect*. 2006;62(2):187-194.
4. Martinez JA, Ruthazer R, Hansjosten K, Barefoot L, Snyderman DR. Role of environmental contamination as a risk factor for acquisition of vancomycin-resistant enterococci in patients treated in a medical intensive care unit. *Arch Intern Med*. 2003;163(16):1905-1912.
5. Bhalla A, Pultz NJ, Gries DM, et al. Acquisition of nosocomial pathogens on hands after contact with environmental surfaces near hospitalized patients. *Infect Cont Hosp Epidemiol*. 2004;25(2):164-167.
6. White LF, Dancer SJ, Robertson C, McDonald J. Are hygiene standards useful in assessing infection risk? *Am J Infect Control*. 2008;36(5):381-384.

7. Huang SS, Datta R, Platt R. Risk of acquiring antibiotic-resistant bacteria from prior room occupants. *Arch Intern Med*. 2006;166(18):1945-1951.
8. Duckro AN, Blom DW, Lyle EA, Weinstein RA, Hayden MK. Transfer of vancomycin-resistant enterococci via health care worker hands. *Arch Intern Med*. 2005;165(3):302-307.
9. Hayden MK, Blom DW, Lyle EA, Moore CG, Weinstein RA. Risk of hand or glove contamination after contact with patients colonized with vancomycin-resistant *Enterococcus* or the colonized patients' environment. *Infect Control Hosp Epidemiol*. 2008;29(2):149-154.
10. Drees M, Snyderman DR, Schmid CH, et al. Prior environmental contamination increases the risk of acquisition of vancomycin-resistant enterococci. *Clin Infect Dis*. 2008;46(5):678-685.
11. Lowe JJ, Gibbs SG, Iwen PC, Smith PW, Hewlett AL. Decontamination of a hospital room using gaseous chlorine dioxide: *Bacillus anthracis*, *Francisella tularensis*, and *Yersinia pestis*. *J Occup Environ Hyg*. 2013;10(10):533-539.
12. Canter DA, Gunning D, Rodgers P, O'Connor L, Traunero C, Kempter CJ. Remediation of *Bacillus anthracis* contamination in the US department of justice mail facility. *Bio Secur Bioterror*. 2005;3(2):119-127.
13. National Research Council. *Reopening Public Facilities After A Biological Attack: A Decision Making Framework*. Washington, DC: National Academies Press; 2005.
14. Boyce JM. New approaches to decontamination of rooms after patients are discharged. *Infect Cont Hosp Epidemiol*. 2009;30(6):515-517.
15. French GL, Otter JA, Shannon KP, Adams NMT, Watling D, Parks MJ. Tackling contamination of the hospital environment by methicillin-resistant *Staphylococcus aureus* (MRSA): a comparison between conventional terminal cleaning and hydrogen peroxide vapour decontamination. *J Hosp Infect*. 2004;57(1):31-37.
16. Otter JA, French GL. Survival of nosocomial bacteria and spores on surfaces and inactivation by hydrogen peroxide vapor. *J Clin Microbiol*. 2009;47(1):205-207.
17. Jeanes A, Rao G, Osman M, Merrick P. Eradication of persistent environmental MRSA. *J Hosp Infect*. 2005;61(1):85-86.
18. Manian FA, Griesenauer S, Senkel D, et al. Isolation of *Acinetobacter baumannii* complex and methicillin-resistant *Staphylococcus aureus* from hospital rooms following terminal cleaning and disinfection: Can we do better? *Infect Cont Hosp Epidemiol*. 2011;32(7):667-672.
19. Carling PC, Parry MM, Rupp ME, Po JL, Dick B, Von Beheren S. Improving cleaning of the environment surrounding patients in 36 acute care hospitals. *Infect Cont Hosp Epidemiol*. 2008;29(11):1035-1041.
20. Otter JA, Yezli S, Perl TM, Barbut F, French GL. The role of 'no-touch' automated room disinfection systems in infection prevention and control. *J Hosp Infect*. 2013;83(1):1-13.
21. Loveday HP, Wilson JA, Pratt RJ, et al. EPIC3: National evidence-based guidelines for preventing healthcare-associated infections in NHS hospitals in England. *J Hosp Infect*. 2014;86:S1-S70.
22. Dancer SJ. Floor wars: The battle for 'clean' surfaces. *J Hosp Infect*. 2013;84(4):339-340.
23. Weber DJ, Rutala WA, Anderson DJ, Chen LF, Sickbert-Bennett EE, Boyce JM. Effectiveness of ultraviolet devices and hydrogen peroxide systems for terminal room decontamination: Focus on clinical trials. *Am J Infect Control*. 2016;44(5):E77-E84.
24. Andersen BM, Rasch M, Hochlin K, Jensen FH, Wismar P, Fredriksen JE. Decontamination of rooms, medical equipment and ambulances using an aerosol of hydrogen peroxide disinfectant. *J Hosp Infect*. 2006;62(2):149-155.
25. Pottage T, Richardson C, Parks S, Walker JT, Bennett AM. Evaluation of hydrogen peroxide gaseous disinfection systems to decontaminate viruses. *J Hosp Infect*. 2010;74(1):55-61.
26. McDonnell G, Russell AD. Antiseptics and disinfectants: Activity, action, and resistance. *Clin Microbiol Rev*. 1999;12(1):147-179.
27. Zonta W, Mauroy A, Farnir F, Thiry E. Virucidal efficacy of a hydrogen peroxide nebulization against murine norovirus and feline calicivirus, two surrogates of human norovirus. *Food Environ Virol*. 2016;8(4):275-282.
28. Passaretti CL, Otter JA, Reich NG, et al. An evaluation of environmental decontamination with hydrogen peroxide vapor for reducing the risk of patient acquisition of multidrug-resistant organisms. *Clin Infect Dis*. 2013;56(1):27-35.
29. Otter JA, Havill NL, Boyce JM. Hydrogen peroxide vapor is not the same as aerosolized hydrogen peroxide. *Infect Cont Hosp Epidemiol*. 2010;31(11):1201-1202.
30. Rogers J, Choi W, Richter W, Stone H, Taylor M. *Bacillus Anthracis* spore inactivation by fumigant decontamination. *Appl Biosaf*. 2008;13:89-98.
31. Beswick AJ, Farrant J, Makison C, et al. Comparison of multiple systems for laboratory whole room fumigation. *Appl Biosaf*. 2011;16(3):139-157.
32. Mitchell BW, Witcher GC, Hammond J. Automated fumigation and neutralization systems for formaldehyde gas. *J Appl Poult Res*. 2000;9(3):359-363.
33. Rogers JV, Choi YW, Richter WR, et al. Formaldehyde gas inactivation of *Bacillus anthracis*, *Bacillus subtilis*, and *Geobacillus stearothermophilus* spores on indoor surface materials. *J Appl Microbiol*. 2007;103(4):1104-1112.
34. Munro K, Lanser J, Flower R. A comparative study of methods to validate formaldehyde decontamination of biological safety cabinets. *Appl Environ Microbiol*. 1999;65(2):873-876.
35. Fink R, Liberman DF, Murphy KIM, Lupo D, Israeli E. Biological safety cabinets, decontamination or sterilization with paraformaldehyde. *Am Indust Hygiene Assoc J*. 1988;49(6):277-279.
36. Lach VH. A study of conventional formaldehyde fumigation methods. *J Appl Bacteriol*. 1990;68(5):471-477.
37. Kim J-G, Yousef AE, Khadre MA. Ozone and Its Current and Future Application in the Food Industry. *Advances in food and nutrition research*. 2003;45:167-218.
38. Rice RG. Ozone and anthrax - knowns and unknowns. *Ozone-Sci Eng*. 2002;24(3):151-158.
39. Gordon G, Rosenblatt AA. Chlorine dioxide: The current state of the art. *Ozone-Sci Eng*. 2005;27(3):203-207.
40. Gibbs SG, Lowe JJ, Smith PW, Hewlett AL. Gaseous chlorine dioxide as an alternative for bedbug control. *Infect Cont Hosp Epidemiol*. 2012;33(5):495-499.
41. Center for Disease Control, Chlorine dioxide. [Online] <https://www.cdc.gov/niosh/idlh/10049044.html>. Accessed June 18, 2014.
42. Center for Disease Control, ToxFAQs - for Formaldehyde. [Online] <https://www.atsdr.cdc.gov/tfacts111.pdf>. Accessed June 18, 2014.
43. OSHA, Hydrogen peroxide in workplace atmospheres, method ID-126-SG. Occupational Safety and Health Administration [Online] <https://www.osha.gov/dts/sltc/methods/partial/t-id126sg-pv-01-0201-m/t-id126sg-pv-01-0201-m.html>. Accessed June 18, 2014.
44. OSHA, OSHA Instruction CPL 02-02-052/ CPL 2-2.52 (REVISED). Occupational Safety and Health Administration: [Online] [https://www.osha.gov/OshDoc/Directive\\_pdf/CPL\\_02-02-052.pdf](https://www.osha.gov/OshDoc/Directive_pdf/CPL_02-02-052.pdf). Accessed June 18, 2014.
45. OSHA, Permissible exposure limits for chemical contaminants. Occupational Safety and Health Administration: [Online] [http://www.dir.ca.gov/title8/5155table\\_ac1.html](http://www.dir.ca.gov/title8/5155table_ac1.html). Accessed June 18, 2014.
46. United States Environmental Protection Agency. Air quality criteria for ozone and related photochemical oxidants; 2006. <http://cfpub.epa.gov/ncea/cfm/recordisplay.cfm?deid=149923> (accessed June 18 2014).
47. Fu TY, Gent P, Kumar V. Efficacy, efficiency and safety aspects of hydrogen peroxide vapour and aerosolized hydrogen peroxide room disinfection systems. *J Hosp Infect*. 2012;80(3):199-205.

48. Puskar MA, Plese MR. Evaluation of real time techniques to measure hydrogen peroxide in air at the permissible exposure limit. *Amer Indust Hygiene Assoc J*. 1996;57(9):843-848.
49. Weschler CJ, Shields HC. Production of the hydroxyl radical in indoor air. *Environ Sci Technol*. 1996;30(11):3250-3258.
50. von Klot S, Wolke G, Tuch T, et al. Increased asthma medication use in association with ambient fine and ultrafine particles. *Eur Respir J*. 2002;20(3):691-702.
51. Pope CA, Burnett RT, Thun MJ, et al. Lung cancer, cardiopulmonary mortality, and long-term exposure to fine particulate air pollution. *JAMA-J Am Med Assoc*. 2002;287(9):1132-1141.
52. Delfino RJ, Zeiger RS, Seltzer JM, Street DH, McLaren CE. Association of asthma symptoms with peak particulate air pollution and effect modification by anti-inflammatory medication use. *Environ Health Persp*. 2002;110(10):A607-A617.
53. Li N, Sioutas C, Cho A, et al. Ultrafine particulate pollutants induce oxidative stress and mitochondrial damage. *Environ Health Persp*. 2003;111(4):455-460.
54. Kowal SF, Allen SR, Kahan TF. Wavelength-resolved photon fluxes of indoor light sources: Implications for HOx production. *Environ Sci Technol*. 2017;51(18):10423-10430.
55. Gomez Alvarez E, Amedro D, Afif C, et al. Unexpectedly high indoor hydroxyl radical concentrations associated with nitrous acid. *Proc Natl Acad Sci USA*. 2013;110(33):13294-13299.
56. Gandolfo A, Gligorovski V, Bartolomei V, et al. Spectrally resolved actinic flux and photolysis frequencies of key species within an indoor environment. *Build Environ*. 2016;109:50-57.
57. Dawe KER, Furlani TC, Kowal SF, Kahan TF, VandenBoer TC, Young CJ. Formation and emission of hydrogen chloride in indoor air. *Indoor Air*. 2019;29(1):70-78.
58. Blocquet M, Guo F, Mendez M, et al. Impact of the spectral and spatial properties of natural light on indoor gas-phase chemistry: Experimental and modeling study. *Indoor Air*. 2018;28(3):426-440.
59. Carslaw N. A new detailed chemical model for indoor air pollution. *Atmos Environ*. 2007;41(6):1164-1179.
60. Kruza M, Lewis AC, Morrison GC, Carslaw N. Impact of surface ozone interactions on indoor air chemistry: A modeling study. *Indoor Air*. 2017;27(5):1001-1011.
61. Carslaw N, Mota T, Jenkin ME, Barley MH, McFiggans G. A significant role for nitrate and peroxide groups on indoor secondary organic aerosol. *Environ Sci Technol*. 2012;46(17):9290-9298.
62. Master Chemical Mechanism. <http://mcm.leeds.ac.uk/MCM/>. Accessed July 17, 2019.
63. Jenkin ME, Saunders SM, Wagner V, Pilling MJ. Protocol for the development of the Master Chemical Mechanism, MCM v3 (Part B): tropospheric degradation of aromatic volatile organic compounds. *Atmos Chem Phys*. 2003;3:181-193.
64. Saunders SM, Pascoe S, Johnson AP, Pilling MJ, Jenkin ME. Development and preliminary test results of an expert system for the automatic generation of tropospheric VOC degradation mechanisms. *Atmos Environ*. 2003;37(13):1723-1735.
65. Bloss C, Wagner V, Jenkin ME, et al. Development of a detailed chemical mechanism (MCMv3.1) for the atmospheric oxidation of aromatic hydrocarbons. *Atmos Chem Phys*. 2005;5:641-664.
66. Jenkin ME, Saunders SM, Pilling MJ. The tropospheric degradation of volatile organic compounds: A protocol for mechanism development. *Atmos Environ*. 1997;31(1):81-104.
67. Wong JPS, Carslaw N, Zhao R, Zhou S, Abbatt JPD. Observations and impacts of bleach washing on indoor chlorine chemistry. *Indoor Air*. 2017;27(6):1082-1090.
68. IUPAC Task Group on Atmospheric Chemical Kinetic Data Evaluation. <http://iupac.pole-ether.fr/>. Accessed July 17, 2019.
69. Nazaroff WW, Cass GR. Mathematical modeling of chemically reactive pollutants in indoor air. *Environ Sci Technol*. 1986;20(9):924-934.
70. Hough AM. The calculation of photolysis rates for use in global tropospheric modelling studies. AERE Report, R-13259, Her Majesty's Stn. Off., Norwich, England. 1988.
71. Sarwar G, Corsi R, Kimura Y, Allen D, Weschler CJ. Hydroxyl radicals in indoor environments. *Atmos Environ*. 2002;36(24):3973-3988.
72. Knibbs LD, Morawska L, Bell SC, Grzybowski P. Room ventilation and the risk of airborne infection transmission in 3 health care settings within a large teaching hospital. *Am J Infect Control*. 2011;39(10):866-872.
73. Currier RP, Torraco DJ, Cross JB, Wagner GL, Gladden PD, Vanderberg LA. Deactivation of clumped and dirty spores of *Bacillus globigii*. *Ozone-Sci Eng*. 2001;23(4):285-294.
74. Davies A, Pottage T, Bennett A, Walker J. Gaseous and air decontamination technologies for *Clostridium difficile* in the healthcare environment. *J Hosp Infect*. 2011;77(3):199-203.
75. Murdoch LE, Bailey L, Banham E, Watson F, Adams NMT, Chewins J. Evaluating different concentrations of hydrogen peroxide in an automated room disinfection system. *Lett Appl Microbiol*. 2016;63(3):178-182.
76. Byrns G, Fuller TP. The risks and benefits of chemical fumigation in the health care environment. *J Occup Environ Hyg*. 2011;8(2):104-112.
77. Ishizaki K, Shinriki N, Matsuyama H. Inactivation of *Bacillus* spores by gaseous ozone. *J Appl Bacteriol*. 1986;60(1):67-72.
78. Burkholder JB, Sander SP, Abbatt J et al. *Chemical Kinetics and Photochemical Data for Use in Atmospheric Studies: Evaluation No. 18*. Pasadena, CA: Jet Propulsion Laboratory, JPL Publication; 2015:15-10.
79. Stone D, Whalley LK, Heard DE. Tropospheric OH and HO<sub>2</sub> radicals: field measurements and model comparisons. *Chem Soc Rev*. 2012;41(19):6348-6404.
80. Li TH, Turpin BJ, Shields HC, Weschler CJ. Indoor hydrogen peroxide derived from ozone/d-limonene reactions. *Environ Sci Technol*. 2002;36(15):3295-3302.
81. Young CJ, Zhou S, Siegel JA, Kahan TF. Illuminating the dark side of indoor oxidants. *Environ Sci-Proc Imp*. 2019;21(8):1229-1239.
82. Carslaw N, Fletcher L, Heard D, Ingham T, Walker H. Significant OH production under surface cleaning and air cleaning conditions: Impact on indoor air quality. *Indoor Air*. 2017;27(6):1091-1100.
83. Axson JL, Washenfelder RA, Kahan TF, Young CJ, Vaida V, Brown SS. Absolute ozone absorption cross section in the Huggins Chappuis minimum (350–470 nm) at 296 K. *Atmos Chem Phys*. 2011;11(22):11581-11590.
84. Voigt S, Orphal J, Bogumil K, Burrows JP. The temperature dependence (203–293 K) of the absorption cross sections of O<sub>3</sub> in the 230–850 nm region measured by Fourier-transform spectroscopy. *J Photochem Photobiol A*. 2001;143(1):1-9.
85. Kahan TF, Washenfelder RA, Vaida V, Brown SS. Cavity-enhanced measurements of hydrogen peroxide absorption cross sections from 353 to 410 nm. *J Phys Chem A*. 2012;116(24):5941-5947.

## SUPPORTING INFORMATION

Additional supporting information may be found online in the Supporting Information section.

**How to cite this article:** Wang Z, Kowal SF, Carslaw N, Kahan TF. Photolysis-driven indoor air chemistry following cleaning of hospital wards. *Indoor Air*. 2020;00:1–15. <https://doi.org/10.1111/ina.12702>